**TITLE PAGE**

# Pharmacological characterization of the αvβ6 integrin binding and internalization kinetics of the foot-and-mouth disease virus derived peptide A20FMDV2.

[1*]Robert J. Slack, [1]Maryam Hafeji, [1]Rebecca Rogers, [2]Steve B. Ludbrook, [3]John F. Marshall, [4]David J. Flint, [4]Susan Pyne, [1]Jane C. Denyer.

[1]Fibrosis and Lung Injury Discovery Performance Unit, Respiratory TAU, GlaxoSmithKline, Gunnels Wood Road, Stevenage, Hertfordshire, UK.

[2]Biological Sciences, Platform Technology & Science, GlaxoSmithKline, Gunnels Wood Road, Stevenage, Hertfordshire, UK.

[3]Centre for Tumour Biology, Barts Cancer Institute, London, United Kingdom.

[4]Strathclyde Institute of Pharmacy and Biomedical Sciences, University of Strathclyde, Glasgow, UK

**Short Title:** A20FMDV2 αvβ6 integrin binding and internalization kinetics

***Author for correspondance:** Robert J. Slack
Fibrosis and Lung Injury DPU
Respiratory TAU
GlaxoSmithKline
Gunnels Wood Road
Stevenage, Hertfordshire, UK SG1 2NY
Phone: +44 1438 762880
Fax: +44 1438 763363
Email: Robert.X.Slack@gsk.com

**Keywords:** αvβ6 integrin, A20FMDV2, latency associated peptide-1, binding kinetics, internalization kinetics

**ABSTRACT**

A20FMDV2 is a peptide derived from the foot-and-mouth disease virus with a high affinity and selectivity for the alpha-v beta-6 (αvβ6) arginyl-glycinyl-aspartic acid (RGD)-binding integrin. It has been shown to be an informative tool ligand in pre-clinical imaging studies for selective labelling of the αvβ6 integrin in a number of disease models. In a radioligand binding assay using a radiolabelled form of the peptide ([$^3$H]A20FMDV2), its high affinity ($K_D$: 0.22 nmol/l) and selectivity (at least 85-fold) for αvβ6 over the other members of the RGD integrin family was confirmed. [$^3$H]A20FMDV2 αvβ6 binding could only be fully reversed in the presence of EDTA whereas a partial reversal was observed in the presence of excess concentrations of an RGD-mimetic small molecule (SC-68448) or unlabelled A20FMDV2. Using flow cytometry on bronchial epithelial cells, the ligand-induced internalization of αvβ6 by A20FMDV2 and $LAP_1$ was shown to be fast ($t_{1/2}$: 1.5 and 3.1 min, respectively), concentration-dependent ($EC_{50}$: values 1.1 and 3.6 nmol/l, respectively) and was followed by a moderately slow return of integrin to the surface. The resultsof the radioligand binding studies suggest that the binding of A20FMDV2 to the RGD binding site on αvβ6 is required to maintain its engagement with the hypothesised A20FMDV2 synergy site on the integrin. In addition, there is evidence from flow cytometric studies that the RGD-ligand engagement of αvβ6 post-internalization plays a role in delaying recycling of the integrin to the cell surface. This mechanism may act as a homeostatic control of membrane αvβ6 following RGD ligand engagement.

## INTRODUCTION

Integrins are heterodimeric, transmembrane glycoprotein receptors that have a primary function to act as signalling proteins in mammals [1]. They are composed of an α and β-subunit, of which in mammals there are 18 and 8 variants, respectively, that can form up to 24 heterodimers [2]. The α and β-subunits are bound in a noncovalent complex and their primary role is to act as adhesion receptors. In order to fulfil this role they have the ability to signal in both directions across the plasma membrane, termed 'inside-out' signalling [3], through binding to extracellular ligands and through cytoplasmic proteins binding to their intracellular domains.

The integrin family is split into sub-families based on a common α or β-subunit or related properties. The arginyl-glycinyl-aspartic acid (RGD) sub-family of integrins share an amino acid binding motif (arginine (R), glycine (G) and aspartic acid (D)) in their endogenous ligands, with selectivity for these ligands determined by their surrounding amino acid sequences [4]. The RGD family of integrins includes the epithelial-restricted integrin alpha-v beta-6 (αvβ6) that was first identified in the early 1990s [5] and which demonstrates a high affinity for fibronectin, tenascin, latency associated peptide-1 ($LAP_1$) and $LAP_3$. In the epithelia of healthy adults, its expression is very low with the exception of the endometrium during the menstrual cycle [5] and diffuse expression associated with subclinical inflammation in the lung and kidney [6]. However, αvβ6 has been identified as being able to activate transforming growth factor-β1 (TGFβ1) by binding to LAP on the constitutively expressed latent TGFβ1 [7]. Upon tissue injury, inflammation and cancer the expression of this integrin is observed to be upregulated significantly. This has been shown in a range of diseases and organs that include acute lung injury and idiopathic pulmonary fibrosis (IPF) in the lung [8,9], fibrosis of the liver and kidney [10,11] and carcinomas of the breast, lung, mouth, skin, colon, stomach and endometrium among others [12]. These observations,

combined with additional data showing αvβ6 inhibition to have positive outcomes in pre-clinical models of fibrosis and cancer [9,10,13], make this integrin a potential therapeutic target for these diseases where the normal control of TGFβ activation has become disrupted.

A20FMDV2 is a 20 amino acid peptide (NAVPNLRGDLQVLAQKVART, fig. 1) derived from the foot-and-mouth disease virus (FMDV) with a high affinity and selectivity for the αvβ6 RGD integrin [14]. It has been shown to be an informative tool ligand in pre-clinical imaging studies for selective labelling of the αvβ6 integrin in a number of disease models [15-17]. Although the high affinity and selectivity of A20FMDV2 has been described previously [14], an accurate determination of its association and dissociation binding kinetics with αvβ6 has not been fully defined and this study addresses this by use of a radiolabelled form of the peptide ([$^{3}$H]A20FMDV2) to characterize these properties. In addition, while it is well established that A20FMDV2 induces internalization of the αvβ6 integrin [15,16], the kinetics of its return to the cell surface following ligand induced internalization is less well described. To further explore this, a flow cytometric assay was developed using normal human bronchial epithelial (NHBE) cells to track αvβ6 location in a primary cell line that also allowed a direct comparison of the effects of A20FMDV2 with those of the endogenous αvβ6 ligand latency associated peptide-1 ($LAP_1$).

## MATERIALS AND METHODS

*Materials*

SC-68448 [18] and cilengitide [19] (fig. 1) were synthesised by the Fibrosis Discovery Performance Unit Medicinal Chemistry group at GSK Medicines Research Centre (Stevenage, UK). Full length LAP$\beta_1$ (fLAP$_1$) (fig. 1) was purchased from Sigma-Aldrich Co. Ltd. (Gillingham, UK). Truncated LAP$\beta_1$ (tLAP$_1$) and the αvβ6 selective peptide NAVPNLRGDLQVLAQKVART (A20FMDV2 derived from the foot-and-mouth disease virus were synthesized by Cambridge Research Biochemicals (Cleveland, UK) (fig. 1). A20FMDV2 was radiolabelled with [$^3$H] by Quotient Bioresearch (Radiochemicals) Ltd. (Cardiff, UK) and had a specific activity of 20 Ci/mmol (incorporation of [$^3$H] determined by mass spectrometry and nuclear magnetic resonance). All other chemicals and reagents were purchased from Sigma-Aldrich Co. Ltd. (Gillingham, UK) unless otherwise stated. NHBE cells, growth medium and supplements were purchased from Lonza (Lonza Group Ltd, Basel, Switzerland). All other cell culture media and reagents were obtained from Invitrogen (Invitrogen Ltd., Paisley, UK). All tissue culture flasks and plates were purchased from Greiner Bio-One (Firckenhausen, Germany) unless otherwise stated. All antibodies used were commercially available and obtained from R&D Systems (Minneapolis, MN, USA) unless otherwise stated and at a stock concentration of 10 μg/ml. These included for flow cytometry phycoerythrin (PE) conjugated mouse IgG2B isotype control (IgG2B-PE) and PE-conjugated mouse monoclonal non-function blocking, anti-human integrin beta-6 (hβ6-PE) and for high content screening (HCS) mouse IgG2B isotype control (IgG2B-HCS), mouse monoclonal anti-human integrin beta-6 (hβ6-HCS) and Alexa Fluor 488 goat IgG anti-mouse Invitrogen (Invitrogen Ltd., Paisley, UK). Cellular assays and radioligand binding assays were completed with a final dimethyl sulphoxide (DMSO) concentration of 0.1% and 1% respectively, unless otherwise stated. Purified soluble protein preparations for

the human integrin proteins αvβ1, αvβ3, αvβ5, αvβ6, αvβ8, α5β1, α8β1 and αIIbβ3 were all purchased from R&D Systems Inc. (Minneapolis, MN, USA) except for α8β1 that was generated by the Biological Sciences department at GSK Medicines Research Centre (Stevenage, UK).

*NHBE Cell Culture*

Frozen aliquots of NHBE cells were placed into culture as a monolayer adhered in type I collagen coated T75 $cm^3$ or T175 $cm^3$ tissue culture flasks using aseptic techniques. Cells were maintained in NHBE cell medium (bronchial epithelial growth medium (BEGM™) containing 0.6 mmol/l $MgCl_2$) supplemented with BEGM™ Clonetics™ SingleQuots (containing bovine pituitary extract, insulin, hydrocortisone, GA-1000 (consisting of 30 mg/ml gentamicin and 15 µg/ml amphotericin), retinoic acid, transferrin, triiodothyronine, epinephrine and human epidermal growth factor)) in 95%:5% air:$CO_2$ at 37ºC and were harvested when ~80% confluent using Accutase®. Cells were then re-suspended in PBS, centrifuged at 300 *g* for 5 min prior to re-suspension in either NHBE cell medium or flow cytometry buffer (RPMI 1640 (without L-glutamine and phenol red) containing 10 mmol/l HEPES, 1% w/v bovine serum albumin (BSA) and 2 mmol/l $MgCl_2$). Cells were then counted on a NucleoCounter NC-3000 (ChemoMetec, Allerød, Denmark) and re-suspended to the required cell density (as detailed beow).

*Radioligand Binding Studies*

All radioligand binding experiments were performed in 96-deep well plates at 37ºC in binding buffer (25 mmol/l 4-(2-hydroxyethyl)-1-piperazineethanesulfonic acid (HEPES), 100 mmol/l NaCl, 2 mmol/l $MgCl_2$ (unless otherwise stated) and 1 mmol/l 3-[(3-cholamidopropyl)dimethylammonio]-1-propanesulfonate (CHAPS) at pH 7.4 (NaOH)). Radioligand binding studies were completed with recombinant soluble integrin proteins in a total volume of 0.5 ml consisting of 50 µl/well of either unlabelled compound at varying

concentrations or vehicle (1% DMSO), 50 µl of [$^3$H]A20FMDV2 and 400 µl/well of purified integrin (0.3 or 2 nmol/l for αvβ6 and 2 nmol/l for αvβ1, αvβ3, αvβ5, αvβ8, α5β1, α8β1 and αIIbβ3).

Non-specific binding (NSB) was determined with either 10 µmol/l SC-68448 (pan-αv small molecule RGD-mimetic [18]), 1 µmol/l A20FMDV2 or 10 mmol/l EDTA (chelating agent). Specific binding was measured by subtracting the NSB from the total radioligand binding in the presence of vehicle (1% DMSO). Plates were incubated with gentle agitation for the time periods indicated and binding terminated by rapid vacuum filtration through a 48-well Brandel harvester (Brandel Inc. Gaithersburg, MD, USA) onto GF/C filter papers pre-soaked in 0.3% v/v poly-ethylenimine. Samples were washed rapidly three times with ice cold distilled water ($dH_2O$) and filters transferred into liquid scintillation (LS) vials containing 4 ml LS fluid (Ultima-Flo™ M, PerkinElmer LAS UK Ltd., Beaconsfield, UK). The amount of radioligand bound to integrin protein was measured by LS spectroscopy using a TriCarb 2900 TR LS counter (PerkinElmer LAS UK Ltd., Beaconsfield, UK).

Association, dissociation and saturation binding studies were performed with [$^3$H]A20FMDV2 to determine radioligand binding kinetics at the human αvβ6 integrin (association rate constant ($k_{on}$), dissociation rate constant ($k_{off}$) and equilibrium dissociation constant ($K_D$) were calculated as described under section 'Data analysis'). For association binding studies, αvβ6 integrin was incubated with varying concentrations of [$^3$H]A20FMDV2 (~0.3 to 2 nmol/l) for varying times up to 2 h prior to filtration. For dissociation binding αvβ6 integrin was pre-incubated for 1 h with a fixed concentration of [$^3$H]A20FMDV2 (~2 nmol/l) before dissociation was initiated by either the addition of an excess of unlabelled compound or 10 mmol/l EDTA before incubation for varying times up to 24 h prior to filtration. For saturation binding αvβ6 integrin protein was incubated with a range of concentrations of [$^3$H]A20FMDV2 (~0.01 to 6 nmol/l) for 6 h prior to filtration. For

RGD integrin selectivity studies 20 nmol/l [$^3$H]A20FMDV2 was incubated for 2 h with purified integrin protein prior to filtration. To demonstrate the divalent cation dependency of integrin binding the specific binding window of a saturating concentration of [$^3$H]A20FMDV2 (~1 nmol/l) was measured against αvβ6 in the absence and presence of a range of concentrations of $Ca^{2+}$, $Mg^{2+}$ and $Mn^{2+}$ following a 4 h incubation.

In order to determine the affinity of integrin ligands for the αvβ6 integrin, competition binding displacement studies were completed where αvβ6 integrin was incubated with a fixed concentration of [$^3$H]A20FMDV2 (~2 nmol/l) and increasing concentrations of unlabelled test ligand for 6 h prior to filtration.

*Flow Cytometric Analysis of αvβ6 Expression*

All flow cytometry assays were performed in 96 well polypropylene microplates with NHBE cells suspended in flow cytometry buffer (45 µl/well with 70,000 cells/well) in the presence of 5 µl/well compound or vehicle (0.1% DMSO). Where stated, cells were permeabilised by incubating with 0.2 % w/v saponin for 5 min at ambient temperature (20-22ºC) prior to compound/vehicle addition. Inhibition of clathrin or lipid raft mediated endocytosis was investigated by pre-incubating NHBE cells with either 2 µg/ml chlorpromazine or 10 µg/ml filipin [20] respectively, for 5 min prior to addition of compound or vehicle (0.1% DMSO). Experiments were stopped by addition of 10 µl/well IgG2B-PE or hβ6-PE and transferring plates to 4$^o$C for 1 h. Plates were then washed twice by centrifuging at 300 *g* for 5 min, removing supernatant and adding flow cytometry buffer (150 µl/well). After the second wash cells were resuspended in flow cytometry buffer (200 µl/well) and cell suspensions transferred into a 96 well round bottom polypropylene plate (Corning Inc. Life Sciences, Tewksbury, MA, USA). Cell samples were then acquired on a fluorescence activated cell sorting (FACS) Canto II (BD Biosciences, San Jose, CA, USA) using a high throughput sampler system and BD FACS Diva™ version 6.1.3 software. Cells

were identified by their forward and side-scatter characteristics and the mean fluorescence intensity of antibody conjugated cells measured. The fluorescence was quantified on at least 5,000 cells and following acquisition all data was exported as flow cytometry standard format 3.0 files with raw data values captured as mean fluorescence intensity (MFI). Fluorescence-activated cell analyses histograms were plotted using FlowJo software (Tree Star Inc. Ashland, OR, USA).

For internalization concentration-response curves NHBE cells were added to 96 well polypropylene microplates containing 5 µl/well compound at varying concentrations or vehicle (0.1% DMSO). Plates were incubated for 2 h in 95%:5% air:$CO_2$ at 37ºC prior to addition of 10 µl IgG2B-PE or hβ6-PE antibody. For determining the rate of ligand-induced αvβ6 internalization NHBE cells were added to 96 well polypropylene microplates containing 5 µl/well compound (at a concentration that caused maximal internalization) or vehicle (0.1% DMSO). Plates were incubated in 95%:5% air:$CO_2$ at 37°C for varying times up to 1 h and then transferred immediately on to ice to stop any further internalization. 10 µl/well IgG2B-PE or hβ6-PE antibody were then added to plates. For determining the rate of αvβ6 return to the cell surface (reversal of ligand-induced αvβ6 internalization), NHBE cells were added to 96 well polypropylene microplates containing 5 µl/well compound (at a concentration that caused maximal internalization) or vehicle (0.1% DMSO). Plates were incubated in in 95%:5% air:$CO_2$ at 37°C for 1 h then centrifuged at 500 *g* for 5 min, supernatant removed and cell pellets re-suspended in PBS (150 µl/well). This process was repeated prior to re-suspension of cells in cell medium (150 µl/well) and incubation for varying times up to 48 h. Plates were then transferred on to ice and 10 µl/well IgG2B-PE or hβ6-PE antibody added. All samples were then processed and read on the FACS Canto II as detailed above.

*Data Analysis*

Analysis of all experiments was completed using GraphPad Prism 5.0 (GraphPad Software, San Diego, CA, USA). In order to allow the results between binding experiments to be averaged, where appropriate, disintegrations per minute (DPM) values were normalized to give the amount (in femtomoles as calculated by the methods preiously described [21]) of radioligand bound per amount (ng) of purified protein (fmol/ng).

Specific binding data from association binding experiments were fitted globally to the association kinetic model (Equation 1, where $K_{ob}$ is the observed rate constant of the association reaction, $k_{on}$ is the association rate constant in units of inverse molar time inverse time ($M^{-1}.min^{-1}$) and $k_{off}$ is the dissociation rate constant in inverse units of time ($min^{-1}$)). From Equation 1 $K_{ob}$ values were subsequently used to calculate association half-life ($t_{1/2}$) values at fixed radioligand concentrations using the equation $t_{1/2} = 0.693/K_{ob}$.

$$K_{ob} = [radioligand] \cdot k_{on} + k_{off} \quad (1)$$

To calculate the percentage of radioligand bound in dissociation binding studies at each time point, Equation 2 was used (where *TB* is total binding of radioligand determined in the presence of vehicle (1% DMSO), *Binding* is the level of binding observed in test well and *NSB* is non-specific binding determined in the presence of either excess unlabelled ligand or EDTA, all measured at the same time point in DPM).

$$\%\ Radioligand\ Bound = \left[\frac{(Binding - NSB)}{(TB - NSB)}\right] \times 100 \quad (2)$$

Dissociation binding data were fitted to a one-phase dissociation model (Equation 3, where $k_{off}$ is the dissociation rate constant in inverse units of time ($min^{-1}$) and $NSB_{t=\infty}$ is non-specific binding determined at infinite time).

$$Binding = (Binding_{t=0} - Binding\ plateau).exp^{(-k_{off}.min)} + NSB_{t=\infty} \quad (3)$$

From Equation 3 $k_{off}$ values were subsequently used to calculate dissociation half-life ($t_{1/2}$) values using the equation $t_{1/2} = 0.693/k_{off}$. Specific binding data from saturation experiments were fitted to a one affinity site model (Equation 4, where $n_H$ is the Hill coefficient and $K$ is the mid-point of the binding isotherm) where appropriate to determine $K_D$. For visualisation only, specific binding data from saturation experiments were also analysed via Scatchard transformation [22] using the method previously described [21].

$$Binding = \frac{B_{max}[radioligand]^{n_H}}{K^{n_H} + [radioligand]^{n_H}} \quad (4)$$

All concentration response curves and competition binding displacement curves were fitted using non-linear regression analysis (four-parameter logistic equation with variable slope [23]) with $EC_{50}$ or $IC_{50}$ values calculated from the fits.

$$\%\ Inhibition\ Binding = \left[\frac{(TB - Binding)}{(TB - NSB)}\right] \times 100 \quad (5)$$

To calculate the percentage inhibition of radioligand binding Equation 5 was used (where *TB* is total binding of radioligand (DPM) determined in the presence of vehicle (1% DMSO), *Binding* is the level of binding observed in DPM at a particular concentration of unlabelled integrin ligand and *NSB* is non-specific binding determined in the presence of 10 µmol/l SC-68448. $IC_{50}$ values generated from competition binding curves against [$^3$H]A20FMDV2 ([$^3$H]A20FMDV2 saturation binding curve $n_H$ = 1) were converted to equilibrium dissociation constant ($K_I$) values using the Cheng-Prusoff equation [24] (Equation 6, where $L^*$ is the radioligand concentration).

$$K_I = \frac{IC_{50}}{1 + \frac{[L^*]}{K_D}} \quad (6)$$

Measurement of the β6 integrin subunit via hβ6-PE binding in flow cytometric assays was used as a surrogate for tracking the location of the αvβ6 heterodimer and for ligand-induced internalization concentration response curves data were expressed as % internalized αvβ6 using Equation 7 (where *x* represents the MFI of hβ6-PE staining in the absence of compound, *y* represents the MFI of hβ6-PE staining in the presence of compound and *z* represents the MFI of isotype control (IgG2B-PE) staining).

$$\%\ Internalised\ \alpha v\beta 6 = \frac{(x-y)}{(x-z)} \times 100 \quad (7)$$

For rates of ligand-induced internalization and subsequent recycling of β6, data were expressed as % αvβ6 surface expression using Equation 8 (where *% αvβ6 SE* is the % αvβ6 surface expression, *x* represents the MFI of hβ6-PE staining in the absence of compound, *y* represents the MFI of hβ6-PE staining in the presence of compound and *z* represents the MFI of isotype control (IgG2B-PE) staining).

$$\%\ \alpha v\beta 6\ SE = 100 - \left( \frac{(x-y)}{(x-z)} \times 100 \right) \quad (8)$$

The ligand-induced β6 internalization data for compounds were fitted to a one-phase decay model (Equation 9, where *% αvβ6 SE* is the % αvβ6 surface expression, $k_{in}$ is the internalization rate constant in inverse units of time ($min^{-1}$) and $\%\ \alpha v\beta 6SE_{t=\infty}$ is % αvβ6 surface expression determined at infinite time). Internalization half-life ($t_{1/2}$) values were calculated using the equation $t_{1/2} = 0.693/k_{in}$.

$$\%\ \alpha v\beta 6\ SE = \left(\%\alpha v\beta 6SE_{t=0} - \%\alpha v\beta 6SE_{plateau}\right).exp^{(-k_{in}.min)} + \%\alpha v\beta 6SE_{t=\infty} \quad (9)$$

For statistical analyses, differences of $p < 0.05$ were considered to be statistically significant. For determination of statistical difference between a single data set and a hypothetical value a one-sample *t*-test was carried out. Statistical significance between two data sets was tested using a Student's unpaired *t*-test. One-way analysis of variance (ANOVA) was used for

comparison of more than two datasets. Unless otherwise indicated, data shown graphically and in the text are either mean ± standard deviation (SD) or, where three or more data points/individual experiments have been completed, mean ± standard error of the mean (SEM).

## RESULTS

*Characterisation of the binding of [$^3$H]A20FMDV2 with the αvβ6 integrin*

In kinetic binding studies the association of [$^3$H]A20FMDV2 to the αvβ6 integrin was measured at ~$K_D$ and 5 x $K_D$ concentrations of radioligand. Global fitting of the association kinetic model to specific association binding data resulted in a $k_{on}$ value of 5.7 ± 0.2 x $10^7$ $M^{-1}.min^{-1}$ (mean ± SEM, n=4) (fig. 2a). The dissociation profiles observed for [$^3$H]A20FMDV2 when initiated by 10 μmol/l SC-68448 or 1 μmol/l A20FMDV2 were comparable and only a partial dissociation of the radioligand was observed (fig. 2b). However, with 10 mmol/l EDTA a single phase dissociation of [$^3$H]A20FMDV2 binding from the αvβ6 integrin was observed with complete dissociation achieved (fig. 2b) with a $t_{1/2}$ of 2.0 ± 0.5 h (mean ± SEM, n=4). Specific binding data from saturation experiments with [$^3$H]A20FMDV2 were fitted to a one affinity site model (with $n_H$) and analysis resulted in the $pK_D$ and $n_H$ values shown in Table 1. The binding to αvβ6 was saturable and high affinity (fig. 2c) with the $n_H$ not significantly different from unity (one-sample *t*-test completed on $\log_{10}$ $n_H$ vs 0, $p > 0.05$) suggesting the binding of [$^3$H]A20FMDV2 to αvβ6 followed the law of mass action at a single site at the range of radioligand concentrations tested in these studies. In addition, no specific binding of [$^3$H]A20FMDV2 was observed to any of the non-αvβ6 RGD integrins investigated (fig. 2d) when tested at ~20 nmol/l radioligand (~100 times [$^3$H]A20FMDV2's αvβ6 $K_D$).

Binding of [$^3$H]A20FMDV2 to αvβ6 required the presence of divalent cations with $Ca^{2+}$, $Mg^{2+}$ and $Mn^{2+}$ able to support binding (fig. 3a). All enabled maximal binding of [$^3$H]A20FMDV2 to αvβ6 however $Mn^{2+}$ was able to support this at much lower concentrations compared with $Mg^{2+}$ and $Ca^{2+}$. In order to determine the affinity of unlabelled RGD-ligands at the αvβ6 integrin under equilibrium conditions, competition displacement binding curves were measured against [$^3$H]A20FMDV2 following a 6 h

incubation period. The $pK_I$ values determined for a range of unlabelled RGD-ligands are summarised in Table 1. All unlabelled ligands inhibited the binding of [$^3$H]A20FMDV2 except the αvβ3/5 selective ligand cilengitide (based on the cyclic peptide cyclo(-RGDfV-) (19)) when tested up to 1 μmol/l. All ligands that did inhibit binding (except $fLAP_1$ against [$^3$H]A20FMDV2 due to the inability to test at concentrations above 50 nmol/l) caused inhibition of radioligand binding to NSB levels (fig. 3b). The $pK_I$ value determined for the unlabelled A20FMDV2 was not significantly different to the $pK_D$ value determined in saturation binding studies with A20FMDV2 (Student's unpaired *t*-test, $p > 0.05$).

*RGD ligand-induced internalization of αvβ6*

To quantitatively measure the surface (membrane) and total (membrane and intracellular pools) NHBE cell expression of αvβ6, flow cytometric assays were completed using hβ6-PE to measure the β6 subunit as a surrogate for the heterodimer (β6 does not pair with any other α integrin subunit). To validate the use of flow cytometry to measure internalization of αvβ6 the endogenous ligand $fLAP_1$ was tested in the absence and presence of 0.2 % w/v saponin to investigate surface and total cell integrin populations respectively. In the absence of saponin a significant reduction in surface expression of the β6 subunit was observed in the presence of $fLAP_1$ (fig. 4a (panel 2) and fig. 4b) (ANOVA, Bonferroni post-test, $p < 0.05$) with MFI values not significantly different from those in the presence of IgG2B-PE isotype control (ANOVA, Bonferroni post-test, $p > 0.05$). When cells were permeabilised in the presence of saponin to allow antibodies intracellular access, there was no significant difference observed between hβ6-PE with and without $fLAP_1$ (ANOVA, Bonferroni post-test, $p > 0.05$) (fig. 4a (panel 4) and fig. 4b). In addition, 0.2 % w/v saponin (concentration used to permeabilise NHBE cells) did not reduce the affinity of $tLAP_1$ for the αvβ6 integrin in a radioligand competition binding assay (data not shown). Based on the MFI values for hβ6-PE in permeabilised (total cell staining) and unpermeabilised (membrane staining)

NHBE cells in the presence of 0.1 % DMSO, ~36% of αvβ6 integrin was present intracellularly and ~64% at the cell surface. The internalization observed in the presence of $fLAP_1$ was significantly inhibited when NHBE cells were pre-incubated with the clathrin-coated pits inhibitor chlorpromazine (ANOVA, Bonferroni post-test, $p < 0.05$) whilst the lipid rafts inhibitor filipin had no effect (fig. 5).

*Kinetics of RGD ligand-induced αvβ6 internalization*

$fLAP_1$ and A20FMDV2 both caused concentration-dependent ligand-induced αvβ6 internalization following a 2 h incubation with NHBE cells (fig. 6a). The $pEC_{50}$ values for internalization of αvβ6 by $fLAP_1$ and A20FMDV2 were 8.45 ± 0.07 and 9.01 ± 0.13 respectively (mean ± SEM, n=4).To determine the rates of ligand-induced internalization the surface expression of αvβ6 was measured over time following the addition of a maximal concentration of $fLAP_1$ or A20FMDV2, as determined in concentration response studies. Both RGD-ligands caused a rapid internalization of αvβ6 ($fLAP_1$ $t_{1/2}$ 3.1 ± 0.8 and A20FMDV2 $t_{1/2}$ 1.5 ± 0.6 min (mean ± SEM, n=4) with no significant difference observed between $t_{1/2}$ (Student's unpaired *t*-test, $p > 0.05$)). A maximal loss of 79% and 80% cell surface integrin was observed for fLAP, and A20FMDV2 respectively, over the 1 h time course studied (fig. 6b). To measure the return of αvβ6 to the surface membrane, washout studies were completed where a maximal concentration of $fLAP_1$ (60 nM) or A20FMDV2 (1 μM) was incubated with NHBE cells for 1 h followed by the removal of αvβ6 ligand and washing of cells in PBS twice. Cells were then incubated for increasing time periods up to 48 h and surface expression of αvβ6 measured at different intervals by flow cytometry. The rate of return of αvβ6 to the cell surface was moderately slow post-washout of both RGD-ligands with 58% and 61% of the total integrin returned to the surface at 48 h still internalized at 4 h (fig. 6b) for A20FMDV2 and $fLAP_1$.

## DISCUSSION

With the FMDV derived peptide A20FMDV2 demonstrating such a high affinity and selectivity for αvβ6, it has been used to great effect as a tool in the cancer field, especially as a radiotracer for *in vivo* imaging studies investigating αvβ6 expression in tumours [14,15]. In this study, A20FMDV2 has been used as tool peptide for comparison with the endogenous αvβ6 ligand $LAP_1$. A number of characteristics of A20FMDV2 demonstrated in previously published studies have been confirmed here with the use of a [$^3$H] labelled form of the peptide. For example, the high affinity and selectivity of A20FMDV2 for the αvβ6 integrin have been confirmed; in addition to this the αvβ6 binding kinetics for the peptide have also been demonstrated. Previously pulished data suggested that A20FMDV2 forms an EDTA-resistant complex with αvβ6, but only if the peptide-integrin complex is pre-formed [25]. It was shown that after 30 min in the presence of an excess of unbiotinylinated A20FMDV2, binding could not be reversed from the pre-formed biotinylated A20FMDV2-αvβ6 complex. For comparison in this study, full dissociation profiles over a 24 h time course were generated for [$^3$H]A20FMDV2, investigating a number of methods to initiate radioligand dissociation. These included the sequestering of divalent metal cations (required for RGD binding [2]) with EDTA and competition with excess unlabelled ligands (both an RGD small molecule binder (SC-68448) and unlabelled A20FMDV2). Over this extended timeframe EDTA was able to reverse the binding of [$^3$H]A20FMDV2 fully. At 30 min no reversal of A20FMDV2 binding to αvβ6 was observed by DiCara and co-workers [25] whereas in this study ~50% of [$^3$H]A20FMDV2 is unbound at this time point. These previously published experiments were completed at 4°C. However, in contrast all binding experiments in this study were completed at 37°C and therefore an explanation for this could be that the slower kinetics at the low temperature conditions resulted in A20FMDV2 dissociation not being detected at the 30 min time point. When dissociation of

[$^3$H]A20FMDV2 from αvβ6 was initiated by either an RGD small molecule RGD-mimetic (SC-68448) or unlabelled A20FMDV2 in this study, only a partial reversal of radioligand binding could be achieved up to 24 h. This may provide further evidence for the so-called "synergy site" that has been proposed for the interaction of RGD-containing peptides with a number of integrins [26, 27], including αvβ6 [28], whereby an interface between the secondary structure of the peptide stabilises the RGD site binding. This is supported by direct competition at the RGD binding site with SC-68448 not being sufficient to fully reverse binding of A20FMDV2 to the αvβ6 integrin. Interestingly, the unlabelled A20FMDV2 is also unable to compete with the second site that may suggest it is not structurally in the correct conformation to achieve this unless first bound to the RGD binding site. In agreement with this suggestion, DiCara and co-workers reported that A20FMDV2 remains unstructured in solution and only assumes 2D and 3D conformation after integrin binding [25]. The full reversal of [$^3$H]A20FMDV2 binding observed with EDTA may suggest that binding of the peptide to both the RGD site and synergy site requires the presence of divalent metal cations. However, it is not clear whether this observation is a result of EDTA having a more efficient inhibition of [$^3$H]A20FMDV2's RGD ligand binding compared with direct competition with an unlabelled RGD-ligand or whether binding to the synergy site itself requires the presence of divalent metal cations. In contrast to the dissociation studies, the association, saturation and competition binding data for [$^3$H]A20FMDV2 shows that if the peptide competes with unlabelled αvβ6 ligands at the same time i.e. is not allowed to form a complex with αvβ6, all the radioligand can be competed off to NSB levels.

The regulation of ligand binding to integrins has been shown to be dependent on divalent cations due to the presence of allosteric cation binding sites within their protein structure [29,30]. Binding of [$^3$H]A20FMDV2 to αvβ6 also required the presence of divalent cations

with $Mn^{2+}$, $Mg^{2+}$ and $Ca^{2+}$ able to support binding. All of these divalent cations were able to support maximal binding of the radiolabelled peptide with αvβ6 although $Mn^{2+}$ was able to achieve this at ~26- and 35-fold lower concentrations compared with $Mg^{2+}$ and $Ca^{2+}$ respectively. The higher potency observed with $Mn^{2+}$ suggested that there was a mixed αvβ6 integrin population in the soluble protein preparation either in the low or high affinity state that could be activated with greater efficiency by this divalent cation [30].

The αvβ3 small molecule RGD-mimetic SC-68448 has been shown in this study to bind to αvβ6 with moderately high affinity, not previously demonstrated, and has provided a useful tool for characterizing the interaction between [$^3$H]A20FMDV2 and αvβ6. This observation suggests that SC-68448 is potentially a pan-αv integrin RGD-mimetic rather than an αvβ3 selective molecule and may provide a useful tool for probing other members of the RGD integrin family. In addition, it has been shown that a truncated version of $LAP_1$ (containing the RGD binding motif and flanking amino acids) has a comparable affinity for the αvβ6 integrin compared with the full length $LAP_1$. Although the $n_H$ for full length $LAP_1$ was steeper (> 1) this is likely a result of being unable to define a complete competition binding curve under the constraints on the highest concentration that could be achieved with the full length protein (50 nmol/l). Therefore, the truncated form of $LAP_1$ also provides an attractive tool for probing the selectivity profile of $LAP_1$ at the other RGD integrins, as concentrations up to high μmol/l could be investigated. This would be extremely useful to understand as it could highlight which other TGFβ activating RGD integrins may be relevant in diseases such as IPF and cancer.

It has been demonstrated that internalization of the integrin occurs following the binding of selective peptides (derived from the human foot-and-mouth virus) to αvβ6 [15,16]. In this study flow cytometry was used to measure the surface expression of αvβ6 and its subsequent loss post-addition of ligand. Although this technique has not been used routinely for

measuring ligand-induced internalization of integrins, it has been used successfully in the G-protein coupled receptor field investigating agonist and antagonist-induced internalization and recycling of the CCR4 receptor [31,32]. A human anti-β6 antibody was used to measure the spatial location of the β6 integrin subunit as a marker for αvβ6. This was chosen in favour of using anti-αvβ6 antibodies as these could bind either orthosterically (at the RGD-site) or allosterically (site distinct from RGD-site) and both would have the potential to compete with αvβ6 ligands. Orthosteric antibodies would also have the potential to induce internalization [33] thus making the measurement of ligand-induced internalization with these antibodies not possible. Even though the antibody used for flow cytometry in this study was designated as anti-β6, it was still confirmed not to bind and compete with the αvβ6 integrin (fig. S1). The inferred ligand-induced internalization observed for $fLAP_1$ in flow cytometry was abolished in the presence of saponin. Saponin permeabilises the plasma cell membrane by forming complexes with cholesterol to generate pores [34] that would allow the antibody to access the intracellular pool of αvβ6. This not only acted as an additional control to confirm $fLAP_1$ was not competing with the anti-β6 antibody but also control data showed the total cell αvβ6 levels relative to the surface level allowing a measurement of intracellular αvβ6, with ~64% of integrin present at the cell surface and ~36% located intracellularly. In addition, it was shown that the αvβ6 internalization in the NHBE system was being driven by a clathrin-dependent mechanism, that agrees with published data where this endocytic mechanism was linked to the αvβ6 integrin [35].

A20FMDV2 demonstrated a higher potency for αvβ6 internalization compared with $fLAP_1$, with a comparable difference to that observed with the affinity estimates in radioligand binding studies. The endogenous internalization and recycling of the αvβ6 integrin has been shown to occur very quickly and within 30 minutes [35,36]. However less is known regarding ligand-induced αvβ6 internalization and the subsequent return of the integrin back

to the cell surface. In this study the rate of internalization was determined for A20FMDV2 and $fLAP_1$ with both shown to internalise αvβ6 very quickly and with comparable $t_{1/2}$ values that were measured within minutes of ligand addition. Furthermore, they both caused a comparable level of αvβ6 internalization (~80% when normalised to isotype control). The more interesting observations in this study were the time of return of αvβ6 post-washout of ligand. Both RGD-peptides post-washout had a comparable profile with ~40 or 50 % (for $fLAP_1$ and A20FMDV2 respectively) of the total integrin returned to the surface at 48 h still internalized at 4 h. The recycling observed in these studies compared with that of endogenous turnover of αvβ6 is slower, suggesting that the internalised ligand-αvβ6 complex return to the cell surface is being delayed by the RGD-ligand interaction. This is comparable to the mechanism by which α5β1 recycling is dependent on the activation state of the integrin [37] as a result of RGD-ligand engagement.

In summary, this study has confirmed A20FMDV2's high affinity and selectivity for αvβ6 using radioligand binding and has shown it exhibits a complex interaction with the integrin post-RGD site binding. The full dissociation of [$^3$H]A20FMDV2 from αvβ6 observed in the presence of EDTA, compared with partial dissociation in the presence of RGD-ligands, suggests either the direct A20FMDV2/αvβ6 synergy site binding requires the presence of metal divalent cations to maintain engagement or it is dependent on the initial RGD-binding site interaction. As it is well established that divalent metal cations are required for RGD site binding it is likely that the latter mechanism is responsible for maintaining the synergy site interface. Therefore, the difference observed between EDTA and direct RGD-ligand competition in dissociation studies is potentially due to removal of metal divalent cations being able to disengage A20FMDV2 from the RGD site fully, whilst RGD-ligands are unable to fully access and dissociate the peptide's RGD interaction post-formation of the tight A20FMDV2-αvβ6 complex.

In conclusion, the internalization of αvβ6 by its endogenous ligand $LAP_1$ has been demonstrated for the first time and its profile is comparable to that observed with A20FMDV2 whereby a fast internalization rate is followed by a moderatley slow return of integrin to the surface. This potentially suggests the RGD-ligand interaction intracellularly plays a role in delaying αvβ6 recycling to the cell surface acting as a mechanism to control subsequent RGD ligand engagement. In addition, this is the first study to characterise the RGD-ligand induced internalization of αvβ6 in normal human epithelial cells that stands as a benchmark for comparison with diseased cells from fibrotic and cancer tissues in future studies.

## ACKNOWLEDGEMENTS

The authors would like to acknowledge Cancer Research Technology for their work in developing A20FMDV2. We would also like to thank the Fibrosis and Lung Injury DPU Medicinal Chemistry group at GlaxoSmithKline for the synthesis of SC-68448.

## AUTHORSHIP CONTRIBUTIONS

*Participated in research design:* Robert J. Slack, John F. Marshall, Steve B. Ludbrook, Jane C. Denyer, David J. Flint, Susan Pyne.

*Conducted experiments:* Robert J. Slack, Maryam Hafeji, Rebecca Rogers.

*Performed data analysis:* Robert J. Slack.

*Wrote or contributed to the writing of the manuscript:* Robert J. Slack, John F. Marshall, Susan Pyne.

## STATEMENT OF CONFLICTS OF INTEREST

The authors have no conflicts of interest to declare.

**REFERENCES**

1. Hynes RO: Integrins: A family of cell surface receptors. Cell 1997; 48:549-554.

2. Hynes RO: Integrins: Bidirectional, allosteric signaling machines. Cell 2002; 110:673-687.

3. Faull RJ, Ginsberg MH: Inside-out signaling through integrins. J Am Soc Nephrol 1996; 7:1091-1097.

4. Ruoslahti E: RGD and other recognition sequences for integrins. Annu Rev Cell Dev Biol 1996; 12:697-715.

5. Busk M, Pytela R, Sheppard D: Characterization of the integrin αvβ6 as a Fibronectin-binding protein. J Biol Chem 1992; 267:5790-5796.

6. Huang XW, Wu JF, Cass D, Erle DJ, Corry D, Young SG et al: Inactivation of the integrin β6 subunit gene reveals a role of epithelial integrins in regulating inflammation in the lungs and skin. J Cell Biol 1996; 133:921-928.

7. Munger JS, Huang X, Kawakatsu H, Griffiths MJ, Dalton SL, Wu J et al: The integrin αvβ6 binds and activates latent TGF β1: a mechanism for regulating pulmonary inflammation and fibrosis. Cell 1999; 96:319-328.

8. Breuss JM, Gallo J, DeLisser HM, Klimanskaya IV, Folkesson HG, Pittet JF, et al: Expression of the β6 integrin subunit in development, neoplasia and tissue repair suggests a role in epithelial remodeling. J Cell Sci 1995; 108:2241-2251.

9. Horan GS, Wood S, Ona V, Jun Li D, Lukashev ME, Weinreb PH et al: Partial inhibition of integrin prevents pulmonary fibrosis without exacerbating inflammation. Am J Respir Crit Care Med 2008; 177:56-65.

10. Popov Y, Patsenker E, Stickel F, Zaks J, Bhaskar KR, Niedobitek G et al: Integrin αvβ6 is a marker of the progression of biliary and portal liver fibrosis and a novel target for antifibrotic therapies. J Hepatol 2008; 48:453-464.

11. Sheppard D: Roles of αv integrins in vascular biology and pulmonary pathology. Curr Opin Cell Biol 2004; 16:552-557.

12. Bandyopadhyay A, Raghavan S: Defining the role of integrin αvβ6 in cancer. Curr Drug Targets 2009; 10:654-652.

13. Eberlein C, Kendrew J, McDaid K, Alfred A, Kang JS, Jacobs VN, Ross SJ, et al: A human monoclonal antibody 264RAD targeting αvβ6 integrin reduces tumour growth and metastasis, and modulates key biomarkers in vivo. Oncogene 2012; 32:4406-4416.

14. Hausner SH, DiCara D, Marik J, Marshall JF, Sutcliffe JL: Use of a peptide derived from foot-and-mouth disease virus for the noninvasive imaging of human cancer: generation and evaluation of 4-[$^{18}$F]Fluorobenzoyl A20FMDV2 for *in vivo* imaging of αvβ6 integrin expression with positron emission tomography. Cancer Res 2007; 67:7833-7840.

15. Hausner SH, Abbey CK, Bold RJ, Gagnon MK, Marik J, Marshall JF, et al: Targeted *in vivo* imaging of integrin αvβ6 with an improved radiotracer and its relevance in a pancreatic tumor model. Cancer Res 2009; 69:5843-5850.

16. Saha A, Ellison D, Thomas GJ, Vallath S, Mather SJ, Hart IR, et al: High-resolution *in vivo* imaging of breast cancer by targeting the pro-invasive integrin αvβ6. J Pathol 2010; 222:52-63.

17. John AE, Luckett JC, Tatler AM, Awais RO, Desai A, Habgood A et al: Preclinical SPECT/CT imaging of αvβ6 integrins for molecular stratification of idiopathic pulmonary fibrosis. J Nucl Med 2013; 54:1-7.

18. Carron CP, Meyer DM, Pegg JA, Engleman VW, Nickols MA, Settle SL et al: A peptidomimetic antagonist of the integrin αvβ3 inhibits leydig cell tumor growth and the development of hypercalcemia of malignancy. Cancer Res 1998; 58:1930-1935.

19. Goodman SL, Hölzemann G, Sulyok GAG, Kessler H: Nanomolar small molecule inhibitors for αvβ6, αvβ5, and αvβ3 integrins. J Med Chem 2002; 45:1045-1051.

20. Ivanov AI: Pharmacological inhibition of endocytic pathways: is it specific enough to be useful? Methods Mol Biol 2008; 440:15-33.

21. Motulsky H, Christopoulos A: Fitting Models to Biological Data using Linear and Nonlinear Regression: A Practical Guide to Curve Fitting; Oxford University Press, New York, 2004.

22. Scatchard G: The attractions of proteins for small molecules and ions. Ann N Y Acad Sci 1949; 51: 660-672.

23. Hill AV: The mode of action of nicotine and curari, determined by the form of the contraction curve and the method of temperature coefficients. J Physiol 1909; 39:361-373.

24. Cheng Y, Prusoff WH: Relationship between the inhibition constant ($K_I$) and the concentration of inhibitor which causes 50 per cent inhibition ($I_{50}$) of an enzymatic reaction. Biochem Pharmacol 1973; 22:3099-3108.

25. DiCara D, Burman A, Clark S, Berryman S, Howard MJ, Hart IR, et al: Foot-and-mouth disease virus forms a highly stable, EDTA-resistant complex with its principal receptor, integrin αvβ6: implications for infectiousness. J Virol 2008; 82:1537-1546.

26. Mardon HJ, Grant KE: The role of the ninth and tenth type III domains of human fibronectin in cell adhesion. FEBS Lett 1994; 340:197-201.

27. Kumar CC, Nie H, Rogers CP, Malkowski M, Maxwell E, Catino JJ et al: Biochemical characterization of the binding of echistatin to integrin αvβ3 receptor. J Pharmacol Exp Ther 1997; 283:843-853.

28. DiCara D, Rapisarda C, Sutcliffe JL, Violette SM, Weinreb PH, Hart IR, et al: Structure-function analysis of Arg-Gly-Asp helix motifs in αvβ6 integrin ligands. J Biol Chem 2007; 282:9657-9665.

29. Lee JO, Bankston LA, Arnaout MA, Liddington RC: Two conformations of the integrin A-domain (I-domain): a pathway for activation? Structure 1995; 3:1333-1340.

30. Plow EF, Haas TA, Zhang L, Loftus J, Smith JW: Ligand binding to integrins. J Biol Chem 2000; 275:21785-21788.

31. Mariani M, Lang R, Binda E, Panina-Bordignon P, D'Ambrosio D: Dominance of CCL22 over CCL17 in induction of chemokine receptor CCR4 desensitization and internalization on human Th2 cells. Eur J Immunol 2004; 34:231-240.

32. Sato T, Iwase M, Miyama M, Komai M, Ohshima E, Asai A et al: Internalization of CCR4 and inhibition of chemotaxis by K777, a potent and selective CCR4 antagonist. Pharmacology 2013; 91:305-313.

33. Weinreb PH, Simon KJ, Rayhorn P, Yang WJ, Leone DR, Dolinski BM: Function-blocking integrin αvβ6 monoclonal antibodies: distinct ligand-mimetic and nonligand-mimetic classes. J Biol Chem 2004; 279:17875-17887.

34. Francis G, Kerem Z, Makkar HP, Becker K: The biological action of saponins in animal systems: a review. Br J Nutr 2002; 88:587-605.

35. Ramsay AG, Keppler MD, Jazayeri M, Thomas GJ, Parsons M, Violette S et al: HS1-associated protein X-1 regulates carcinoma cell migration and invasion via clathrin-mediated endocytosis of integrin αvβ6. Cancer Res 2007; 67:5275-5284.

36. Wang J, Wu J, Hong J, Chen R, Xu K, Niu W et al: PKC promotes the migration of colon cancer cells by regulating the internalization and recycling of integrin αvβ6. Cancer Lett 2011; 311:38-47.

37. Dozynkiewicz MA, Jamieson NB, Macpherson I, Grindlay J, van den Berghe PV, von Thun A et al: Rab25 and CLIC3 collaborate to promote integrin recycling from late endosomes/lysosomes and drive cancer progression. Dev Cell 2012; 22:131-45.

**FIGURE LEGENDS**

**Fig.1.** Chemical structures of the RGD ligands used in this study.

**Fig.2.** Characterisation of [$^3$H]A20FMDV2 αvβ6 integrin binding and RGD integrin selectivity. **a** Association binding kinetics of [$^3$H]A20FMDV2 to the human αvβ6 integrin. **b** Dissociation binding kinetics of [$^3$H]A20FMDV2 from the human αvβ6 integrin. Dissociation was initiated by either addition of 10 μM SC-68448, 1 μM A20FMDV2 or 10 mmol/l EDTA following a 1 h pre-incubation of [$^3$H]A20FMDV2 with αvβ6. **c** Saturation binding of [$^3$H]A20FMDV2 to the human αvβ6 integrin. **d** [$^3$H]A20FMDV2 binding selectivity for the RGD integrins. Radioligand binding was measured by liquid scintillation spectroscopy using 0.3 (**a**, **b** and **c**) or 2 (**d**) nmol/l αvβ6 and 2 nmol/l for non-αvβ6 RGD integrins. For RGD selectivity and saturation binding studies plates were incubated for 4 or 6 h respectively. Specific binding (**a**, **c** and **d**) was determined from total and non-specific binding values measured in the presence of vehicle (1% DMSO) and 10 μmol/l SC-68448 respectively. Data shown in **a**, **b** and **c** are the mean ± SD of duplicate points and are representative of four individual experiments with similar results. Data shown in **d** are the mean ± SEM of four individual experiments carried out in quadruplicate.

**Fig.3.** Divalent cation dependency of [$^3$H]A20FMDV2 human αvβ6 integrin binding and αvβ6 competition displacement binding curves. **a** Specific binding of [$^3$H]A20FMDV2 to the human αvβ6 integrin in the presence of increasing $Ca^{2+}$, $Mg^{2+}$ and $Mn^{2+}$. **b** Competition displacement binding curves for integrin ligands against [$^3$H]A20FMDV2 with the human αvβ6 integrin. Radioligand binding was measured by liquid scintillation spectroscopy using 0.3 nmol/l αvβ6 and either ~1 (**a**) or 2 (**b**) nmol/l [$^3$H]A20FMDV2 following a 4 (**a**) or 6 (**b**) h incubation. Specific binding was determined from total and non-specific binding values measured in the presence of vehicle (1% DMSO) and 10 μmol/l SC-68448 respectively, and were used to calculate the % inhibition of radioligand bound to the αvβ6 integrin. Data

shown are the mean ± SEM of at least four individual experiments carried out in singlicate (**b**) or duplicate (**a**).

**Fig.4.** Ligand-induced αvβ6 internalization triggered by $fLAP_1$ in NHBE cells. **a** Flow cytometry histograms showing $fLAP_1$-induced αvβ6 internalization. β6 integrin staining was determined by flow cytometry where NHBE cells were washed and stained, either with (panels 3 and 4) or without (panels 1 and 2) permeabilization (with or without 0.2% w/v saponin), with either a PE-conjugated mouse IgG2B isotype control (white histogram), PE-conjugated mouse monoclonal anti-human integrin β6 (hβ6-PE) (black histogram) or the latter in the presence of 60 nmol/l $fLAP_1$ (grey histogram). Control experiments were completed in the presence of 0.1% DMSO with all conditions tested following a 2 h incubation. Specific mean fluorescence intensity (MFI) values are shown in each panel in bold (geometric mean ± SEM of four individual experiments) and were calculated by subtracting the MFI of the negative isotype control from the anti-β6 stained samples. **b** Flow cytometry MFI plots showing $fLAP_1$-induced αvβ6 internalization. Significant differences between test groups denoted by ** $p < 0.01$ or * $p < 0.05$ (ANOVA, Bonferoni's post-test). Data shown in **a** are representative of four individual experiments with similar results. Data shown in **b** are the geometric mean ± SEM of four individual experiments carried out in duplicate.

**Fig.5.** Effect of clathrin-coated pits and lipid rafts disrupting agents on $fLAP_1$-induced αvβ6 internalization. Inhibition of clathrin or lipid raft mediated endocytosis was investigated by pre-incubating NHBE cells with either 2 μg/ml chlorpromazine or 10 μg/ml filipin respectively, for 5 min prior to addition of $fLAP_1$ or control (0.1% DMSO) for a 2 h incubation. β6 integrin staining was then determined by flow cytometry where NHBE cells were washed and stained with either a PE-conjugated mouse IgG2B isotype control (IgG2B-PE) or PE-conjugated mouse monoclonal anti-human integrin β6 (hβ6-PE). Significant

differences between test groups denoted by ** $p < 0.01$ (ANOVA, Bonferoni's post-test). Data shown are the mean ± SEM of three individual experiments carried out in duplicate. ns, not significant.

**Fig. 6.** RGD ligand-induced internalization and surface repopulation kinetics of the αvβ6 integrin in NHBE cells. **a** Internalistion concentration response curves were generated by incubating compounds at a range of concentrations with NHBE cells for 2 h prior to the measurement of the β6 integrin subunit at the cell surface in a flow cytometric assay. **b** Single concentrations of $fLAP_1$ (60 nmol/l) or A20FMDV2 (10 μM) were used to induce αvβ6 internalization at 37ºC. To investigate the kinetics of internalization, plates were transferred on to ice at different time points post-compound addition and the β6 integrin subunit at the cell surface measured in a flow cytometric assay. To measure the return of the αvβ6 integrin to the surface post-ligand-induced internalization, NHBE cells were exposed to RGD-ligand for 1 h and then washed twice with PBS and additionally incubated at 37ºC for various time points up to 48 h. In flow cytometric assays NHBE cells were washed and stained with either PE-conjugated mouse IgG2B isotype control (IgG2B-PE) or PE-conjugated mouse monoclonal anti-human integrin β6 (hβ6-PE) at the time points indicated. Ligand-induced internalization data in **a** were normalised using the mean fluoresecence intensity (MFI) values for the IgG2B-PE and hβ6-PE in the presence of 0.1% DMSO and expressed as % internalised αvβ6. For kinetic studies in **b** data were normalised using the MFI values for IgG2B-PE and hβ6-PE in the presence of vehicle (0.1% DMSO) at each time point and expressed as % αvβ6 surface expression. Data shown are the mean ± SEM of four individual experiments carried out in duplicate.

**Table 1** The affinity of RGD-ligands for the human αvβ6 integrin determined from [$^3$H]A20FMDV2 saturation and competition binding studies.

| **Ligand** | $K_D/K_I$ (μmol/l) | $pK_D/pK_I$ | $n_H$ |
|---|---|---|---|
| **[$^3$H]A20FMDV2** | *0.22 ± 0.07 | *9.77 ± 0.08 | 1.20 (0.96, 1.44) |
| **A20FMDV2** | 0.24 ± 0.06 | 9.62 ± 0.05 | 0.89 (0.67, 1.12) |
| **SC-68448** | 12.3 ± 4.21 | 8.34 ± 0.28 | 1.00 (0.87, 1.14) |
| **tLAP$_1$** | 0.50 ± 0.12 | 8.54 ± 0.12 | 1.01 (0.81, 1.22) |
| **fLAP$_1$** | 1.05 ± 0.16 | 9.00 ± 0.08 | 1.83 (0.56, 3.11) |
| **Cilengitide** | <122 | <6.92 | N/A |

Data shown are mean values ± S.E.M. for at least four separate determinations. $pK_D$, negative $\log_{10}$ of $K_D$; $pK_I$, negative $\log_{10}$ of $K_I$; $n_H$, Hill slope; *denotes $K_D/pK_D$; N/A, not applicable.

## SUPPLEMENTARY DATA

## SUPPLEMENTARY MATERIALS AND METHODS

*αvβ6 Mediated Cell Adhesion*

The myelogenous leukemia K562 cell line (S1) stably expressing the αvβ6 integrin (K562-αvβ6) was generated by the Biological Sciences Department at GSK Medicines Research Centre (Stevenage, UK) using previously described methods (S2). K562-αvβ6 cells were cultured as a suspension in T175 tissue culture flasks using aseptic techniques in equal volumes of Roswell Park Memorial Institute (RPMI) 1640 and Dulbecco's Modified Eagle's Medium (DMEM) containing 10 % heat inactivated fetal calf serum (FCS), 2 mmol/l glutamine and 1 mg/ml geneticin in 95 %:5 % air:$CO_2$ at 37ºC. Glutathione S-transferase fusion LAP-TGFβ-1 (GST-$LAP_1$) protein (generated as previously described (S2), corresponding to the RGD integrin-binding domain of $LAP_1$ (amino acids 242-252 – GRRGDLATIHG), was coated (100 µl/well) onto 96-well MaxiSorp® flat-bottom plates (Thermo Fisher Scientific, MA, USA) at a concentration of 100 µg/ml and incubated for 2 h at 37ºC. Plates were then washed twice with 200 µl/well PBS after which blocked with 3 % w/v BSA in PBS (100 µl/well) for 1 h. Plates were then washed twice with 200 µl/well PBS and 25 µl/well of cell adhesion assay buffer (Hank's balanced salt solution (HBSS) containing 25 mM HEPES) containing 8 mM $MgCl_2$ was added. Test antibodies (mouse IgG2A isotype control (IgG2A), mouse IgG2B isotype control (flow unconjugated IgG2B) (both generated by BioPharm Research and Development department at GSK Medicines Research Centre (Stevenage, UK)), mouse monoclonal anti-human integrin beta-6 (flow unconjugated anti-β6) (R&D Systems, Minneapolis, MN, USA) and RGD-mimetic blocking monoclonal anti-human integrin αvβ6 clone 10D5 (10D5 anti-αvβ6) (Merck Millipore, Billerica, MA, USA)) were made up in cell adhesion assay buffer (0.4 % DMSO to give a final DMSO concentration of 0.1 %) and added to plates (25 µl/well). K562-αvβ6 cells were

re-suspended to 0.25 or 3 x $10^6$ cells/ml respectively, and 2',7'-bis-(2-carboxyethyl)-5-(and-6)-carboxyfluorescein, acetoxymethyl ester (BCECF-AM) added to give a final concentration of 5 μmol/l prior to a 10 min incubation at 37ºC. K562-αvβ6 cells (0.15 x $10^6$ cells/well with 50 μl/well) were then added to plates (giving a final $MgCl_2$ concentration of 2 mM) prior to a 30 min incubation at 37ºC. Plates were then washed twice with 200 μl/well PBS and 50 μl/well 0.5 % Triton X-100 detection solution added. Following a 5 min incubation at ambient temperature (20-22ºC) fluorescence (relative light units) was measured (excitation wavelength 485 nm and emission wavelength 535 nm) using an EnVision® multilabel plate reader (PerkinElmer LAS UK Ltd., Beaconsfield, UK). In order to average data between separate experimental determinations in the K562-αvβ6 assay format, data were normalised within experiments using a positive (10 mM EDTA) and negative control (0.1 % DMSO).

**SUPPLEMENTARY FIGURE LEGEND**

**Fig.S1.** β6 flow cytometry antibodies do not inhibit αvβ6 cell adhesion to GST-$LAP_1$. The effect of blocking and unconjugated flow cytometry β6 antibodies (including isotype controls) on αvβ6 cell adhesion was measured by incubating antibodies at 100 μg/ml with K562 cells recombinantly expressing the αvβ6 integrin in plates coated with GST-$LAP_1$. Plates were incubated for 30 min prior to removal of non-adhering cell populations and the remaining adhered cells were then quantified by fluorescence using BCECF-AM. Total and non-specific binding values were measured in the presence of vehicle (1 % DMSO) and 10 mM EDTA respectively, and were used to calculate the % inhibition of cell adhesion. Data shown are the mean ± SEM of at least four individual experiments carried out in singlicate.

**SUPPLEMENTARY REFERENCES**

S1. Lozzio CB, Lozzio BB: Human chronic myelogenous leukemia cell-line with positive Philadelphia chromosome. Blood 1975; 45:321-34.

S2. Ludbrook SB, Barry ST, Delves CJ, Horgan CM: The integrin αvβ3 is a receptor for the latency-associated peptides of transforming growth factors β1 and β3. Biochem J 2003; 369:311-18.

Fig. 1

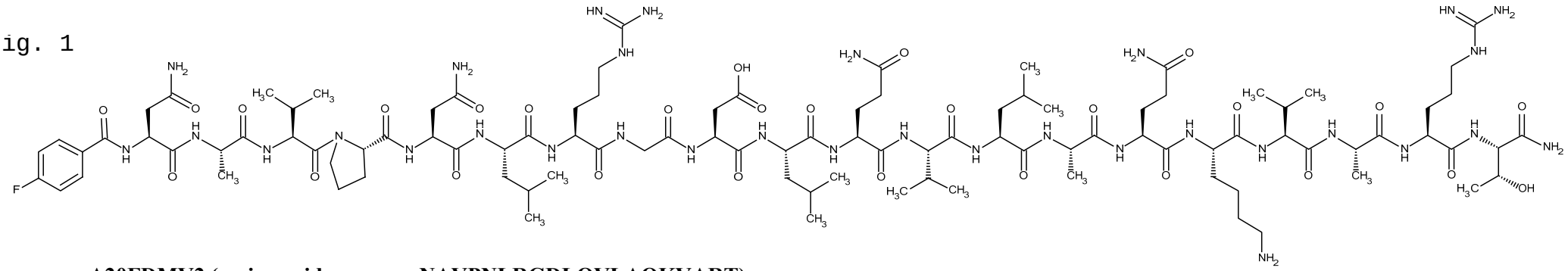

**A20FDMV2 (amino acid sequence NAVPNLRGDLQVLAQKVART)**

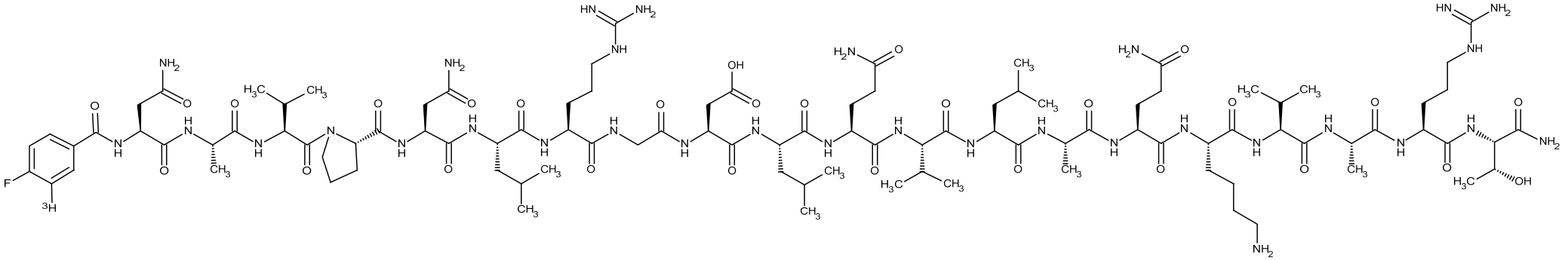

**[$^3$H]A20FDMV2 (amino acid sequence NAVPNLRGDLQVLAQKVART)**

LSTCKTIDMELVKRKRIEAIRGQILSKLRLASPPSQGEVPPGPLPEAVLALYNSTRDRVAGESA
EPEPEPEADYYAKEVTRVLMVETHNEIYDKFKQSTHSIYMFFNTSELREAVPEPVLLSRAELR
LLRLKLKVEQHVELYQKYSNNSWRYLSNRLLAPSDSPEWLSFDVTGVVRQWLSRGGEIEGF
RLSAHCSCDSRDNTLQVDINGFTTGR**RGD**LATIHGMNRPFLLLMATPLERAQHLQSSRHRR

**Full length TGF$\beta_1$ latency associated peptide (fLAP$_1$) amino acid sequence (RGD integrin binding sequence in bold)**

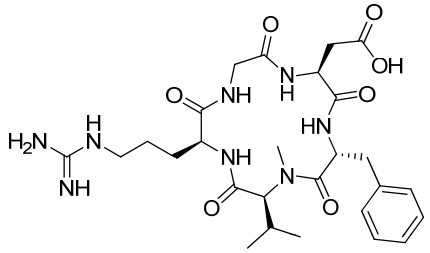

**Cilengitide**

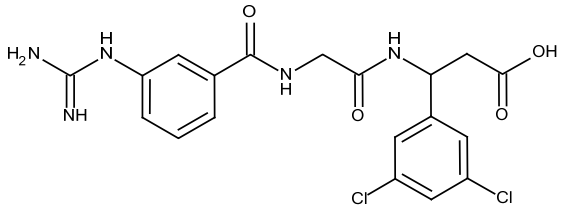

**SC-68448**

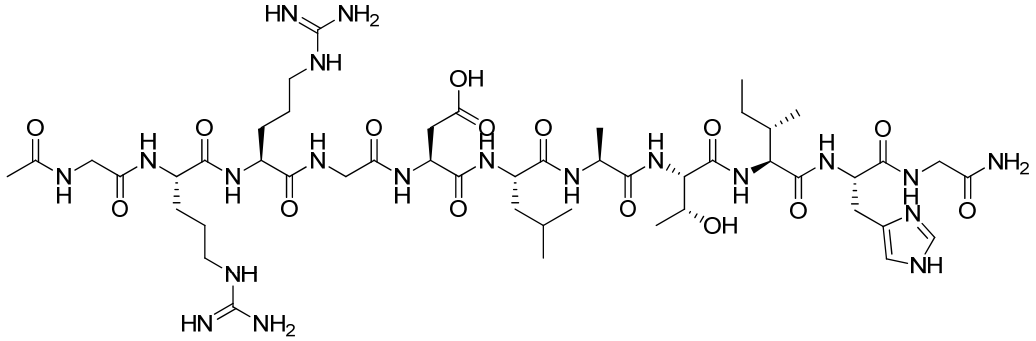

**Truncated TGF$\beta_1$ latency associated peptide (tLAP$_1$) (amino acid sequence GRRGDLATIHG)**

Fig. 2

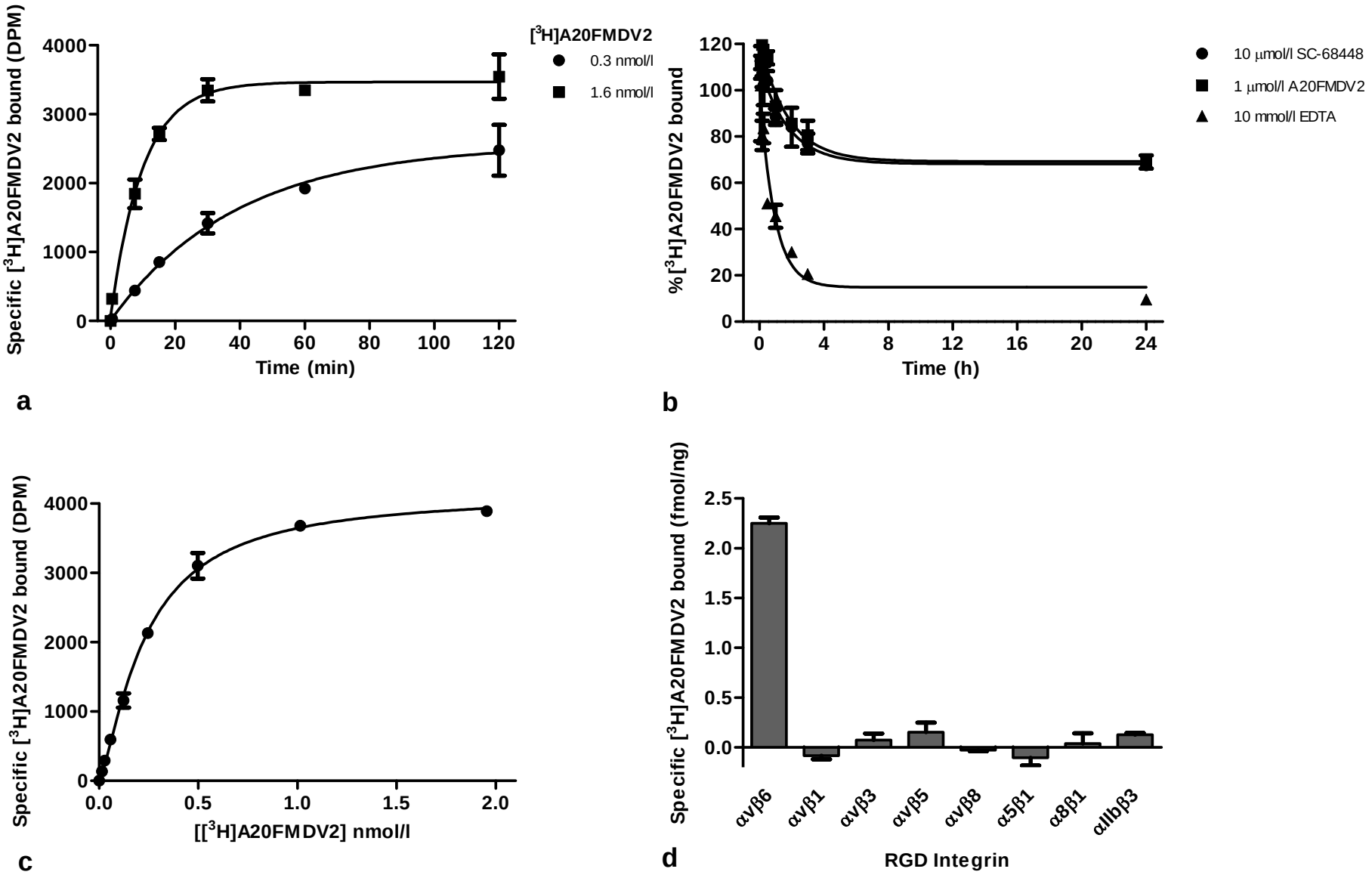
Specific [3H]A20FMDV2 bound (DPM)
4000
3000
2000
1000
0
0
20
40
60
80
100
120
Time (min)
[3H]A20FMDV2
0.3 nmol/l
1.6 nmol/l
a
%[3H]A20FMDV2 bound
120
100
80
60
40
20
0
0
4
8
12
16
20
24
Time (h)
10 µmol/l SC-68448
1 µmol/l A20FMDV2
10 mmol/l EDTA
b
Specific [3H]A20FMDV2 bound (DPM)
4000
3000
2000
1000
0
0.0
0.5
1.0
1.5
2.0
[[3H]A20FMDV2] nmol/l
c
Specific [3H]A20FMDV2 bound (fmol/ng)
2.5
2.0
1.5
1.0
0.5
0.0
αvβ6
αvβ1
αvβ3
αvβ5
αvβ8
α5β1
α8β1
αIIbβ3
RGD Integrin
d

Fig. 3

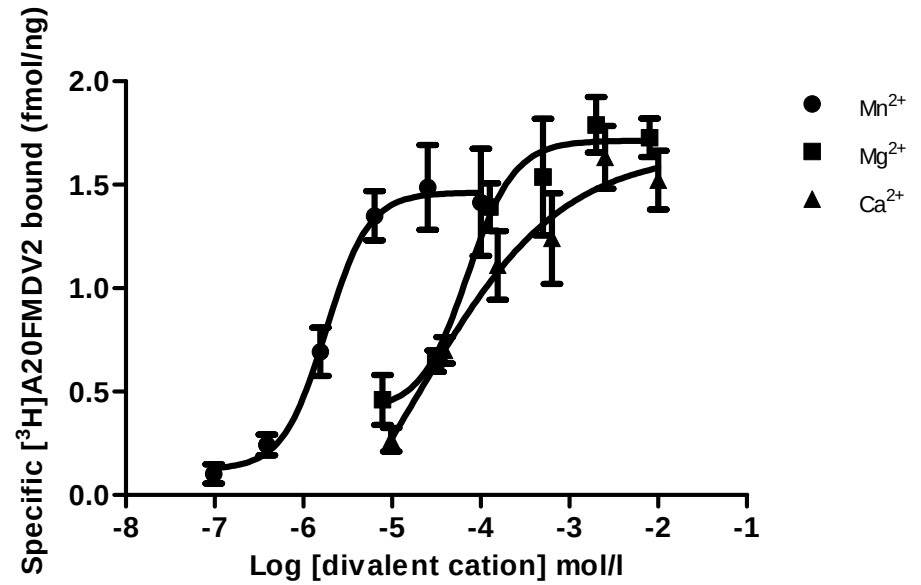
Specific [3H]A20FMDV2 bound (fmol/ng)
2.0
1.5
1.0
0.5
0.0
-8
-7
-6
-5
-4
-3
-2
-1
Log [divalent cation] mol/l
Mn2+
Mg2+
Ca2+

a

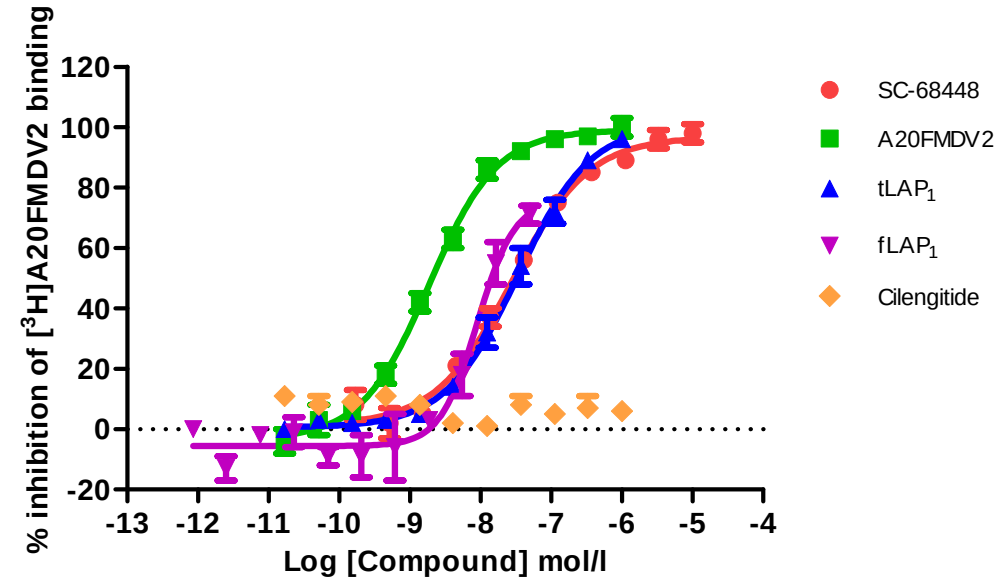
% inhibition of [3H]A20FMDV2 binding
120
100
80
60
40
20
0
-20
-13
-12
-11
-10
-9
-8
-7
-6
-5
-4
Log [Compound] mol/l
SC-68448
A20FMDV2
tLAP1
fLAP1
Cilengitide

b

Fig. 4

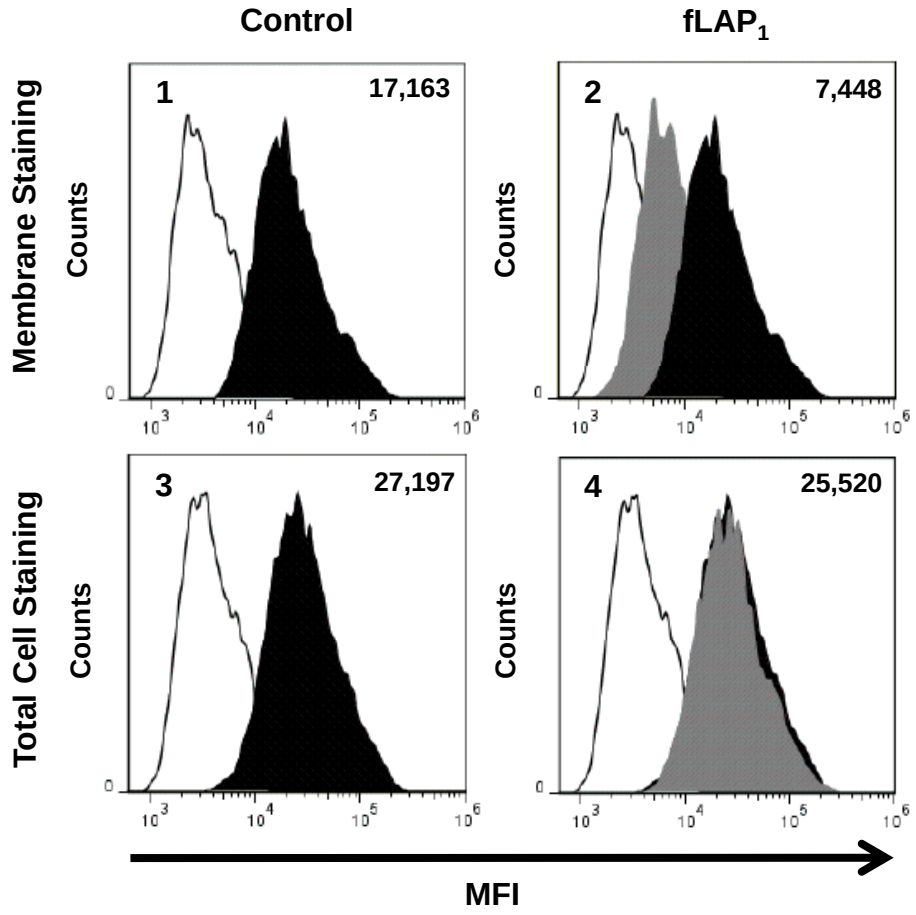
Control
fLAP1
Membrane Staining
Total Cell Staining
Counts
1
17,163
2
7,448
3
27,197
4
25,520
MFI

a

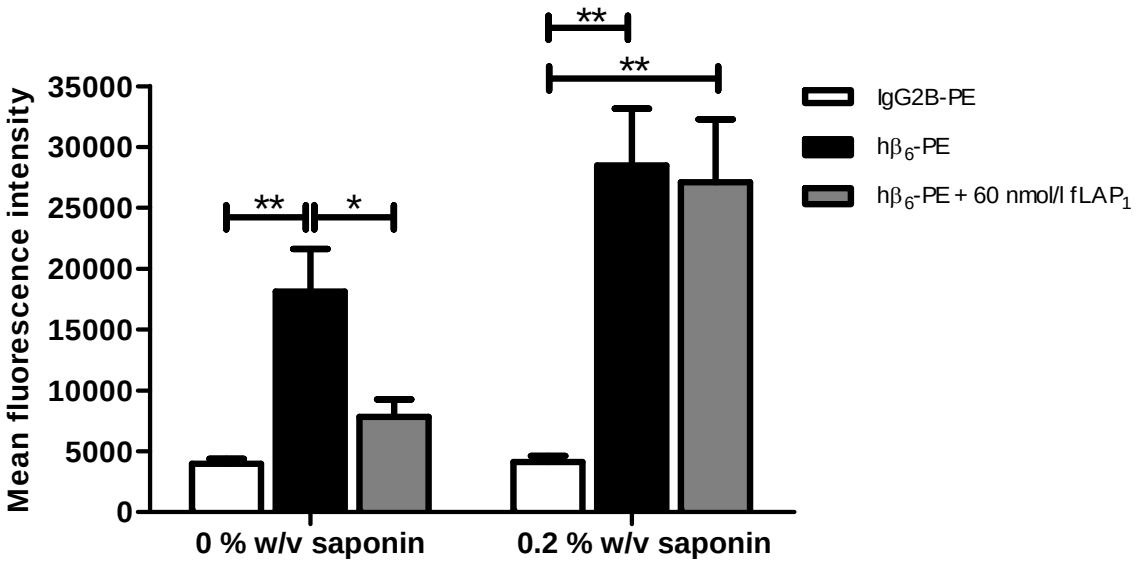
Mean fluorescence intensity
35000
30000
25000
20000
15000
10000
5000
0
**
*
**
**
0 % w/v saponin
0.2 % w/v saponin
IgG2B-PE
hβ6-PE
hβ6-PE + 60 nmol/l fLAP1

b

Fig. 5

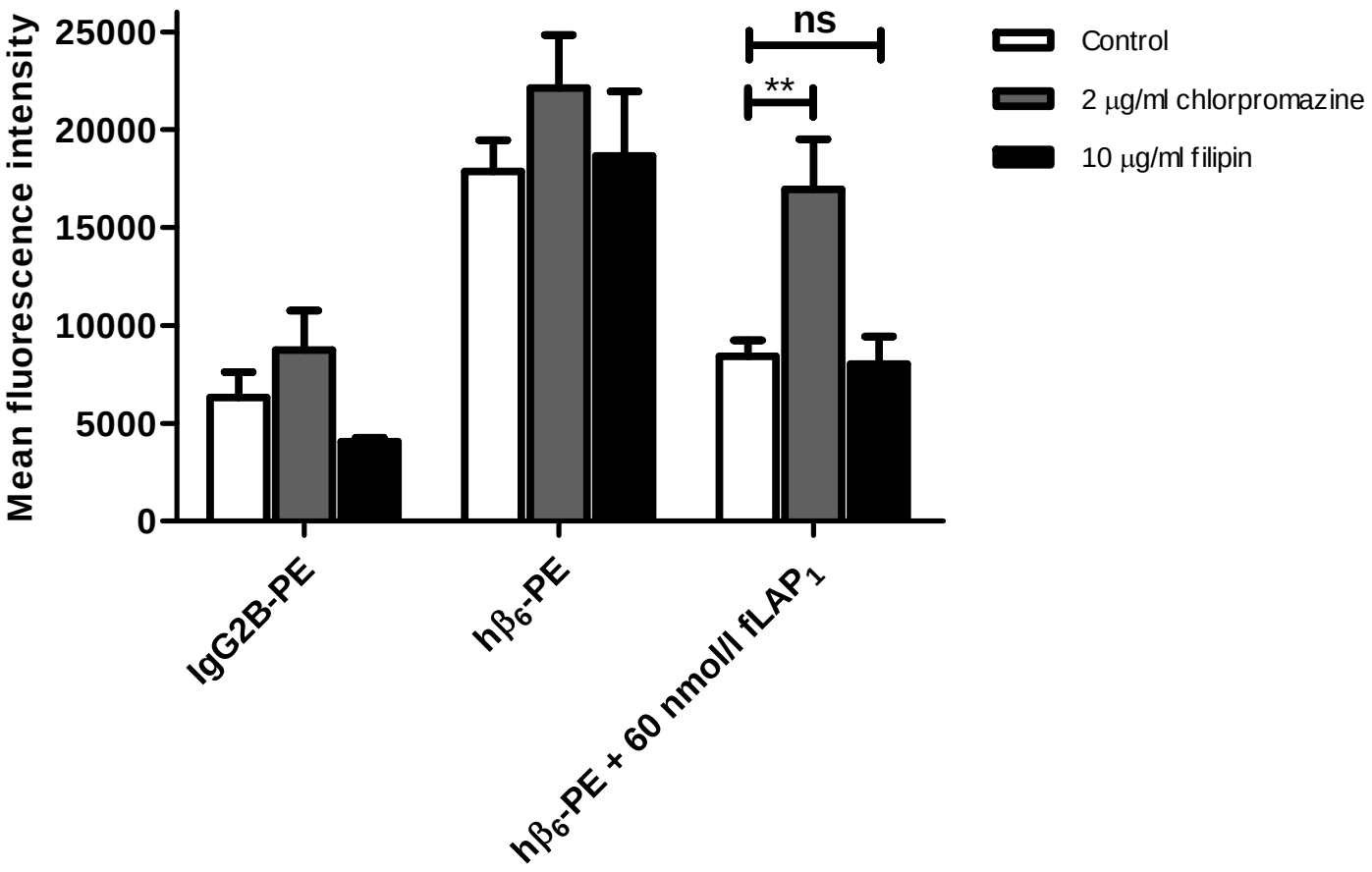
Mean fluorescence intensity
25000
20000
15000
10000
5000
0
ns
**
Control
2 μg/ml chlorpromazine
10 μg/ml filipin
IgG2B-PE
hβ6-PE
hβ6-PE + 60 nmol/l fLAP1

Fig. 6

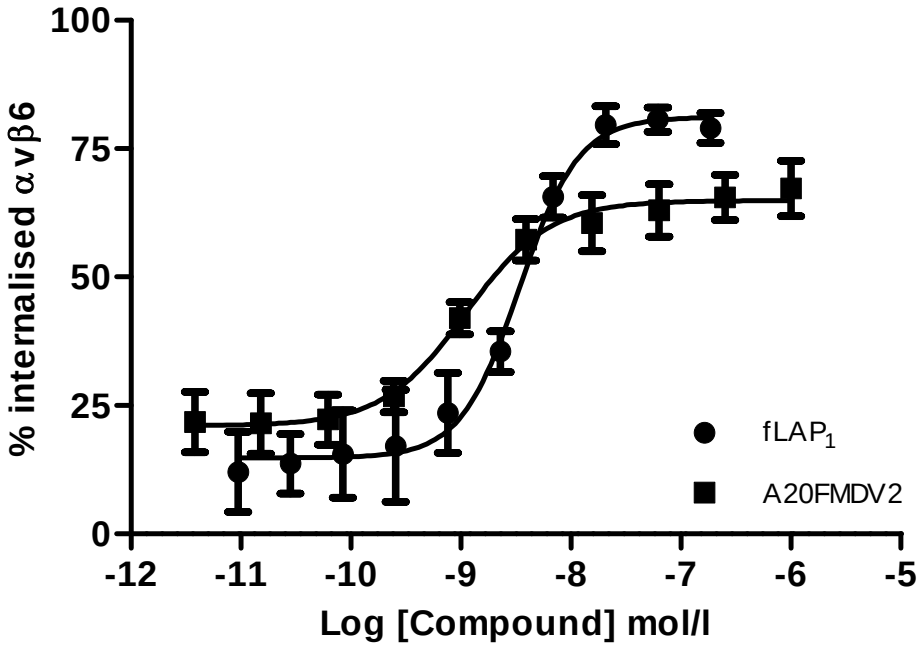
100
75
50
25
0
% internalised αvβ6
-12
-11
-10
-9
-8
-7
-6
-5
Log [Compound] mol/l
fLAP1
A20FMDV2

a

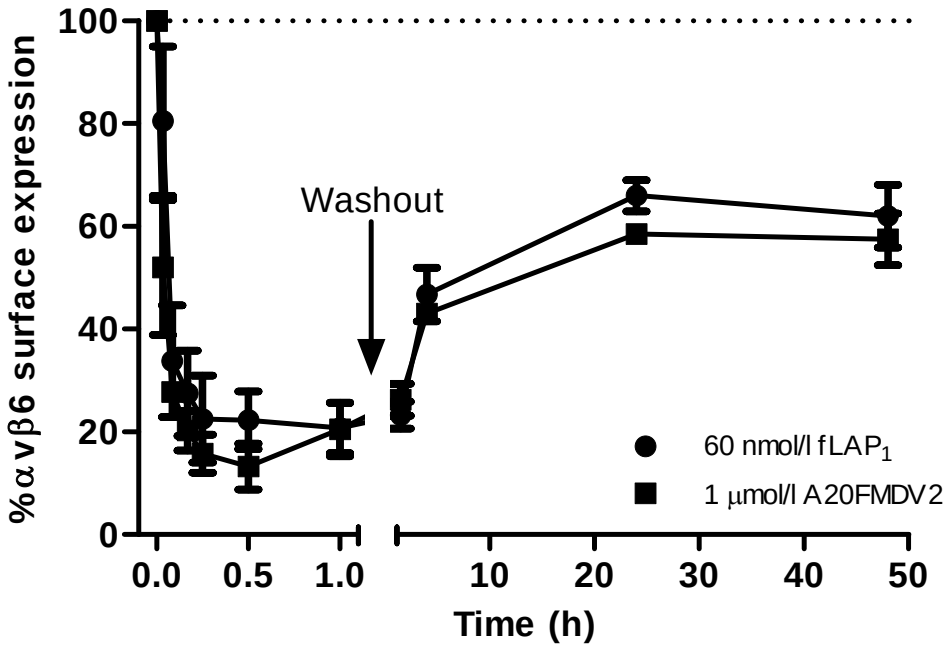
100
80
60
40
20
0
% αvβ6 surface expression
Washout
0.0
0.5
1.0
10
20
30
40
50
Time (h)
60 nmol/l fLAP1
1 μmol/l A20FMDV2

b

Fig. S1

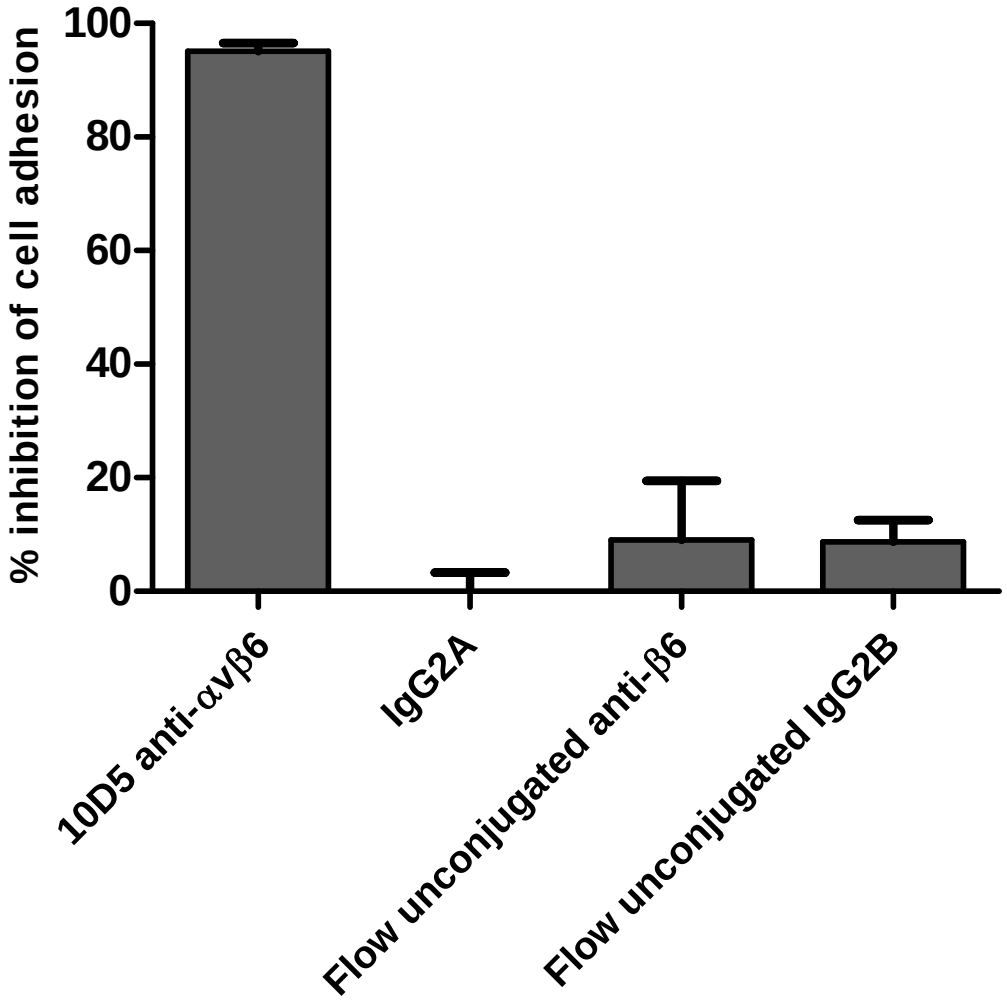
% inhibition of cell adhesion
100
80
60
40
20
0
10D5 anti-αvβ6
IgG2A
Flow unconjugated anti-β6
Flow unconjugated IgG2B